TWENTYFIFTH EUROPEAN ROTORCRAFT FORUM

Paper n° H9

PREDICTION OF THE OFF-AXIS RESPONSE TO CYCLIC PITCH USING A MANEUVERING FREE WAKE MODEL

BY

COLIN THEODORE
ROBERTO CELI
UNIVERSITY OF MARYLAND, COLLEGE PARK, USA

SEPTEMBER 14-16, 1999
ROME
ITALY

ASSOCIAZIONE INDUSTRIE PER L'AEROSPAZIO, I SISTEMI E LA DIFESA
ASSOCIAZIONE ITALIANA DI AERONAUTICA E ASTRONAUTICA

PREDICTION OF THE OFF-AXIS RESPONSE TO CYCLIC PITCH USING A MANEUVERING FREE WAKE MODEL

Colin Theodore[1]
Roberto Celi[2]
Department of Aerospace Engineering
Glenn L. Martin Institute of Technology
University of Maryland, College Park, USA

Abstract

This paper presents a study on the effect of wake modeling on the prediction of the off-axis response to pilot inputs for a hingeless and an articulated rotor helicopter, including a comparison with flight test data. The free wake model can capture geometry changes due to maneuvering flight. The prediction of the response to pilot inputs improves only slightly; in particular, the off-axis response is still predicted in the wrong direction. The effects due to wake geometry have the correct direction, but they are weak. Key discrepancies between simulation and test develop after less than one half rotor revolution following the maneuver, when body rates are negligible and therefore the wake geometry has not changed appreciably. The mechanism causing these initial discrepancies remains unclear, and appears to be related to angular accelerations, rather than rates. If wake geometry is important, a relaxation type free wake might not be appropriate, and an unsteady free wake may be necessary.

Notation

j_{max}	Number of blade azimuthal steps in one revolution
k_{max}	Vortex segment end points in discretized wake
p, q, r	Roll, pitch and yaw rates of the helicopter
$\vec{r}$	Position vector of a point on a vortex filament
u, v, w	Helicopter velocity components along body axes
u	Control vector
$\vec{V}$	Local velocity vector of a point
$\vec{V}_e$	External velocity vector at a point
$\vec{V}_{ind}$	Wake induced velocity vector at a point
$\vec{V}_\infty$	Free stream velocity vector
$\mathbf{X}_{trim}$	Vector of trim variables
y	State vector
α_F, β_F	Angles of attack and sideslip of the fuselage
$\Delta\psi$	Azimuthal discretization resolution
$\Delta\zeta$	Vortex filament discretization resolution
ζ	Distance along vortex filament
θ_0, θ_{0t}	Collective pitch setting of the main and tail rotors
θ_{1s}, θ_{1c}	Main rotor longitudinal and lateral cyclic pitch settings
θ_F, ϕ_F, ψ_F	Pitch, roll and yaw attitudes of the helicopter
$\lambda_0, \lambda_{1c}, \lambda_{1s}$	Main rotor dynamic inflow coefficients
λ_{0t}	Tail rotor inflow
ξ	Vector of truncated Fourier series coefficients
ψ	Blade azimuth angle

Introduction

In recent years, the need for a reliable design of flight control systems has prompted interest in improving the accuracy of flight dynamics mathematical models of helicopters. This has especially led to a more sophisticated modeling of the rotor system, both from the dynamic and the aerodynamic point of view. Particular attention has been given to one long standing problem in flight dynamic modeling, namely the prediction of the off-axis response to pilot input, and especially of pitch and roll cross-coupling. Until recently, the predictions of the off-axis response (e.g., the pitch response to a lateral cyclic pitch input) were inaccurate to the point of sometimes having the wrong sign, compared to the results of flight tests. The cause for the discrepancies has eluded the helicopter flight dynamics community for many years.

The first major contribution to the understanding of the off-axis response problem has come from Rosen and Isser [1, 2], who have attributed the prediction errors to the incorrect modeling of the geometry of the main rotor wake during pitch and roll maneuvers. Pitch and roll motion reduce the spacing of the wake vortices on one side of the rotor disk, and increase it on the opposite side. This change in wake geometry modifies the inflow distribution at the rotor disk, causes changes in blade flapping, and in turn changes in pitch and roll moments. Taking into account these geometry changes through a specially developed prescribed wake model improved the prediction of cross-coupling pitch and roll derivatives for the UH-60 and the AH-64.

Following Rosen and Isser's work, other investigators have developed simple inflow models that capture the inflow changes due to a maneuver through the use of correction coefficients. Keller [3] and Arnold *et al.* [4] have developed an extended momentum theory that contains simple additional inflow terms proportional to pitch and roll rates. The additional terms contain correction coefficients, the numerical values of which are determined based on a simplified vortex wake analysis. Significant improvements were obtained for the prediction of the

[1]Graduate Research Assistant, Alfred Gessow Rotorcraft Center; e-mail: colint@eng.umd.edu.

[2]Associate Professor, Alfred Gessow Rotorcraft Center; e-mail: celi@eng.umd.edu.

off-axis response of the UH-60. The traditional dynamic inflow model has been extended by Krothapalli *et al.* [5] to include pitch and roll motions.

The wake geometry changes due to a maneuver have also been modeled by Basset [6, 7] using a dynamic vortex wake model. In this model the wake is represented by vortex rings; geometry and vorticity evolve dynamically as a function of rotor airloads and motion. Substantial improvements in the prediction of the hover off-axis response for the BO-105 were obtained.

A completely different explanation for the discrepancies of off-axis predictions has been offered by von Grünhagen [8]. The agreement can be improved by including a "virtual inertia effect" associated with the swirl in the rotor wake. This results in simple correction terms that can be added to a dynamic inflow theory, and that improve considerably the off-axis predictions for a BO-105.

All the previous studies attempt to improve the correlation of off-axis response through refined theoretical models. A different approach has been proposed by Mansur and Tischler [9]. Corrected lift and drag coefficients of the blade airfoils are obtained from the instantaneous, baseline values through a first-order filter, the time constant of which is selected in terms of an equivalent aerodynamic phase lag. This phase lag is then determined from flight test data using system identification techniques. More recently, the phase lag has also been determined using the simulation model of Refs. [1, 2].

Finally, a free wake model that can capture the wake distortions due to pitch and roll rates has been recently developed by Bagai *et al.* [11]. From the point of view of the present study, the most important feature of this wake model is that no *a priori* assumptions are required for the wake geometry. The geometry is determined by the convection of the vortex filaments in the induced velocity field, and takes rigorously into account the kinematics of the maneuver.

The main objectives of this paper are:

1. To describe a refined flight dynamic simulation model, obtained by coupling a nonreal-time simulation model which includes rotor blade flexibility with the maneuvering free wake of Ref. [11]; and

2. To present results obtained using the refined model for the hover response to pilot inputs, including comparisons with flight test data for the BO-105 and the UH-60 helicopters. Special emphasis will be given to the prediction of the off-axis response.

Brief Review of Flight Dynamics Model

The flight dynamic model is described in detail Refs. [12], [13] and [14], and only a brief summary of the main features will be presented here. The simulation model is based on a first-order non-linear state-space representation of the equations of motion. The rigid body dynamics of the helicopter is modeled using non-linear Euler equations. The aerodynamics of the fuselage and of the horizontal and vertical tail are taken into account in the form of lookup tables. These lookup tables are presented as a function of the angle of attack and angle of sideslip of the fuselage. Since they are obtained through wind tunnel tests, they are valid for a wide range of angles of attack and sideslip. Three Euler rate equations are added which relate the derivatives of the Euler angles to the roll, pitch, and yaw rates of the helicopter. The rotor model describes the dynamics of each blade in flap, lag, and torsion. The blade equations are written to take into account arbitrary hub motions and the blade elastic deformations need not be small (within the limit of the validity of the Euler angles used for fuselage dynamics). By combining the rigid body fuselage equations with the blade dynamics equations, the result is a system of first-order coupled differential equations for the rotor and fuselage. When the free wake is not used, rotor wake dynamics is modeled using a three-state dynamic inflow model [15]. A one state dynamic inflow model is used for the tail rotor.

Brief Review Of Wake Model

The free wake model coupled with the flight dynamics code is the Bagai-Leishman free wake model (Ref. [11]). The main characteristic of this free wake model from the point of view of a flight dynamics simulation is that it can model distortions of the wake geometry during a maneuver. The essence of the Leishman-Bagai free wake analysis is that the rotor wake is discretized into a number of straight line vortex segments. The ends of each of these vortex segments are called collocation points and the set of these points describes the geometry of the rotor wake. The number of straight line vortex segments used to model a vortex filament trailing behind each rotor blade is given by the vortex filament discretization resolution, $\Delta\zeta$, and the total length of the trailed vortex considered in the analysis. The total length of the trailed vortex filament is given by the number of rotor revolutions from the time that the filament was first generated and is a measure of the total wake age.

The overall geometry of the free wake is characterized by the positions of the collocation points corresponding to a number of trailed vortex filaments, each of which is generated at a discrete azimuth angle. The spacing of the discrete azimuth angles around the rotor disk is constant and this spacing is called the azimuthal discretization resolution, $\Delta\psi$. It is not necessary in the free wake code for the azimuthal discretization resolution, $\Delta\psi$, to be equal to the vortex filament discretization resolution, $\Delta\zeta$, but they are equal for this coupling with the flight dynamics code. The bound circulation is an input to the free wake code and is given at a number of radial blade segments at each azimuth angle considered. The number of blade segments is arbitrary; they do not have to be of equal length along the span. The bound circulation is

assumed to be constant over each individual blade segment. It should be mentioned that the Leishman-Bagai free wake code used in this analysis has provision for rigid near-wake trailers to be released along the span of the blade, but the current analysis only makes use of the tip-vortex capability.

The free wake model is characterized as a relaxation wake model. A model of this type is governed by the vorticity transport equation [16]

$$\frac{d\vec{r}(\psi,\zeta)}{dt} = \vec{V}(\vec{r}(\psi,\zeta)) \tag{1}$$

This equation states that a particle in the flow field is convected with the local velocity at that point. Here $\vec{r}(\psi,\zeta)$ is the position vector of the point on the vortex filament that was generated by a blade at the azimuth angle, ψ, and is an azimuthal distance, ζ, behind the blade. $\vec{V}(\vec{r}(\psi,\zeta))$ is the local velocity vector at the point $\vec{r}(\psi,\zeta)$. This local velocity vector is the sum of the effects of the induced velocity resulting from the circulation of the wake vortices as well as the bound circulation from the rotor blades, plus any free stream and maneuver contributions. The velocity is given by[16]

$$\vec{V}(\vec{r}(\psi,\zeta)) = \vec{V}_\infty + \vec{V}_e(\vec{r}(\psi,\zeta)) + \vec{V}_{ind}(\vec{r}(\psi,\zeta)) \tag{2}$$

Here $\vec{V}_\infty$ is the free stream velocity which is uniform over the entire flow-field. $\vec{V}_e(\vec{r}(\psi,\zeta))$ is an external velocity profile that results from outside influences such as gusts and maneuvers. This external velocity profile is a function of the position of the point as the velocity profile is generally not uniform through the flow field, as in pitch and roll rate maneuvers.

The calculation of the wake geometry is performed using a pseudo-implicit predictor-corrector numerical method (Ref. [16]). An iterative process is involved in calculating the rotor wake geometry for a given bound circulation distribution. An initial wake geometry is used to start the iterative process. With each iteration the geometry of the free wake is changed according to the pseudo-implicit predictor-corrector equations so a new wake geometry is generated. The convergence criteria for the wake geometry is based on the L_2 norm of the change in wake geometry between successive iterations. The root mean square (RMS) change in the wake structure is calculated using [16]:

$$RMS = \frac{1}{j_{max}k_{max}}\sqrt{\sum_{\psi:j=1}^{j_{max}}\sum_{\zeta:k=1}^{k_{max}}(\vec{r}^{\,n}_{j,k} - \vec{r}^{\,n-1}_{j,k})^2} \tag{3}$$

where j_{max} is the number of blade azimuthal steps in one revolution and k_{max} is the number of collocation points used to describe each of the trailed vortex filaments.

In the free wake model, the wake geometry iterative process is started using an undistorted helical wake. The RMS change in the wake geometry on the first iteration is used as the basis of the convergence criteria. The wake geometry is considered converged when the ratio of the RMS change for the current iteration to the RMS change of the first iteration falls below a certain threshold[16]:

$$\epsilon > \frac{(RMS)_n}{(RMS)_1} \tag{4}$$

where $(RMS)_n$ is the RMS change in wake geometry of the nth iteration, $(RMS)_1$ is the RMS change of the first iteration and ϵ is the threshold for convergence.

The assumption is made in the analysis for this paper that the tip vortex release point is at the blade tip. The initial strength of the vortex released from the blade at a particular azimuth angle is equal to the value of the maximum bound circulation along the blade at that azimuth angle. There is provision in the free wake code to have the tip vortex released from the point of maximum bound vorticity or the centroid of vorticity, but neither of these options is exercised in the present study.

Finally, the converged wake is used to calculate the local induced velocity at specified points along the blades and around the azimuth. These local velocities only contain contributions from the bound and wake circulations and represent only the induced velocity, $\vec{V}_{ind}(\vec{r}(\psi,\zeta))$ from Eq. 2. The free stream and maneuver velocity contributions are included internally in the flight dynamics code.

Incorporation of free wake calculations in trim procedure

The basic trim procedure used in this study is essentially the same as that described in Refs. [17] and [12]. This is a coupled rotor-fuselage trim procedure for a helicopter in a coordinated steady turn. For a given helicopter configuration the flight condition is defined by the velocity V along the trajectory, the flight path angle γ, and the turn rate $\dot{\psi}$. Straight horizontal flight is treated as a special case with zero turn rate and flight path angle.

The vector $\mathbf{X}$ of unknowns of the baseline trim procedure is

$$\begin{aligned}\mathbf{X}_{trim} = [&\theta_0\ \theta_{1c}\ \theta_{1s}\ \theta_{0t}\ \alpha_F\ \beta_F\ \theta_F\ \phi_F \\ &q_0^1\ q_{1c}^1\ q_{1s}^1\ q_{2c}^1\ q_{2s}^1 \cdots q_{nc}^1\ q_{ns}^1 \cdots \\ &\cdots q_0^m\ q_{1c}^m\ q_{1s}^m\ q_{2c}^m\ q_{2s}^m \cdots q_{nc}^m\ q_{ns}^m \\ &\lambda_0\ \lambda_{1c}\ \lambda_{1s}\ \lambda_{0t}]\end{aligned} \tag{5}$$

Therefore, the unknowns of the baseline trim procedure include the collective pitch θ_0, lateral and longitudinal cyclic pitch θ_{1c} and θ_{1s}, and tail rotor collective θ_{0t}; the angles of attack α_F and sideslip β_F of the fuselage; and the pitch and roll Euler angles θ_F and ϕ_F of the fuselage. As in Ref. [17], a modal coordinate transformation is performed to reduce the number of degrees of freedom

of the blade model. The generalized coordinates for each flap, lag, or torsion mode are expanded in a truncated Fourier series, and the coefficients of the expansions become unknowns of the trim problem. With reference to Eq. (6), q_0^k is the constant coefficient in the expansion for the k-th blade mode, and q_{jc}^k and q_{js}^k are respectively the coefficients of the j-th harmonic cosine and sine for the k-th mode. All the results obtained in the present paper were obtained with just one flap mode; three harmonics were retained in the expansion of the modal coefficient. Therefore, the modeling of the steady-state position of the blade required seven trim unknowns in the vector $\mathbf{X}$, for a total of 19 trim variables.

The trim problem is defined by a set of coupled nonlinear algebraic equations [17, 18] that enforce three force and three moment equilibrium along and about the aircraft body axes; three kinematic relationships between roll, pitch and yaw rates and turn rate; one equation enforcing turn coordination; and one kinematic condition on the flight path angle.

At this point, it is important to discuss the differences between the dynamic inflow and free wake models with respect to trim. For the three-state dynamic inflow model considered in this paper, there are three additional trim variables added to the trim vector. The induced velocity at any point of the rotor disk is calculated using the dynamic inflow equation,

$$\lambda(r,\psi) = \lambda_0 + \lambda_{1c}\frac{r}{R}\cos\psi + \lambda_{1s}\frac{r}{R}\sin\psi \qquad (6)$$

where λ_0 represents the uniform component and λ_{1c} and λ_{1s} represent the linear variation in inflow in the longitudinal and lateral directions over the rotor disk. Thus using the dynamic inflow model, the inflow is calculated for a given blade azimuth angle, ψ, and radial station, r.

The free wake model does not introduce any additional trim variables into the trim vector as the dynamic inflow model does. Thus the total number of trim variables is lower when the free wake model is used in favor of the dynamic inflow model. With the inclusion of the free wake model, the inflow is calculated using the Biot-Savart law from the geometry and circulation characteristics of the free wake, as well as the bound circulation distribution [16]. Using the Biot-Savart equation, the inflow can be calculated at any point in the flow field and used in the flight dynamics code.

The inputs to the free wake code include: the advance ratio; the distribution of bound circulation; the displacements of the blades (both rigid and elastic); the tip vortex release points and initial strengths; and the angles of attack and sideslip at the rotor hub. The bound circulation at a particular blade station and azimuth angle is calculated in the flight dynamics code from the following equation:

$$\Gamma_b = \frac{1}{2}C_L V c \qquad (7)$$

where Γ is the bound circulation per unit span, C_L is the local lift coefficient, V is the local velocity and c is the local blade chord. The lift coefficient is formulated using quasi-steady aerodynamics and is obtained from look-up tables for a given angle of attack and Mach number.

The blade displacement distribution is given by

$$w(r,\psi) = \sum_{i=1}^{NM} \phi^{(i)}(r)\xi^{(i)}(\psi) \qquad (8)$$

where NM is the number of normal modes, $\phi^{(i)}$ is the ith normal mode, $\xi^{(i)}$ is the modal coefficient for the ith mode at a given azimuth angle and $w(r,\psi)$ is the deflection of the blade section at a given azimuth angle and blade radial station. Using the deflection, w, the position of the point in the hub fixed axis system is calculated. The hub fixed axis system is used by the free wake code for the wake calculations. The flight dynamics code supplies a table of blade section positions where the bound circulation is calculated and where the inflow is to be calculated by the free wake code.

The tip vortex release points and initial vortex strengths are also supplied to the free wake code. In the current analysis, the tip vortices are released at the blade tip. The initial strength of the tip vortex at a given azimuth angle is assumed to be the maximum value of the bound circulation at that particular azimuth angle.

The advance ratio and angles of attack and sideslip at the hub are used in the free wake code to calculate the free stream velocity, $\vec{V}_\infty$, in Eq. (2). The pitch and roll rates are used in the free wake code to calculate the external velocity profile, $\vec{V}_e(\vec{r}(\psi,\zeta))$, applied to the rotor wake. The inclusion of the free wake model in the trim procedure involves an iterative process on the bound circulation distribution from the flight dynamics code and the inflow distribution from the free wake code. The blade displacements are not an explicit part of this iteration since they are calculated from the normal modes and the modal coefficients and do not depend directly on the inflow or the bound circulation distributions.

The circulation-inflow iteration is started in the flight dynamics code by assuming an initial inflow distribution. This inflow is used in the flight dynamics code aerodynamic model to calculate the blade aerodynamic loading, including the bound circulation distribution over the rotor disk. This bound circulation is fed into the free wake code that produces the inflow distribution when the wake has converged. This inflow is then used in the flight dynamics code to calculate the bound circulation distribution to continue the iterative process. This inflow-circulation iteration is considered converged when the change in L_2 norm between successive iterations falls below a certain threshold.

The first time the free wake is run the starting wake geometry is an undistorted helical wake structure. However, each additional time the free wake code is run the initial wake geometry is the final geometry from the

previous run. Thus the original convergence criteria, Eq. (4), which is based on the first geometry change, is not appropriate here since the starting wake geometry will be different each time. The new free wake convergence criteria uses the RMS change in the wake geometry for the current iteration, but without the normalization of the RMS change on the first iteration. The wake geometry is considered converged when the RMS change falls below a certain threshold, as follows:

$$\epsilon > (RMS)_n \tag{9}$$

The trim procedure with the free wake model included is characterized by three nested loops as follows:

- The outermost loop involves the iterative process of solving the system of coupled non-linear algebraic equations. This is done through the application of a standard non-linear equation solver. This solver first calculates a finite difference approximation to the Jacobian matrix and then iterates on the trim vector, X_{trim}, to find the trim solution.

- The second iterative loop is on the circulation and inflow distributions that has already been described. Each step of the iteration involves running the free wake code. The result of this loop is a converged inflow distribution that is used in the aerodynamic portions of the trim equations.

- The innermost loop is the iteration on the tip vortex geometries in the free wake code. The result of this loop is a converged wake that is used to calculate the inflow distribution.

Results

The results presented in this section refer to two helicopters, namely the Eurocopter BO-105 and the Sikorsky UH-60, both with the flight control system turned off (bare airframe configuration). The BO-105 has a single main rotor with a hingeless sort in-plane main rotor configuration. This hingeless configuration results in a high relative hinge offset of about 14%, which produces a high control power and bandwidth, making the helicopter highly maneuverable. This high relative hinge offset also contributes to high cross couplings between the longitudinal and lateral-directional dynamics of the helicopter. The UH-60 has an articulated rotor with a hinge offset of 4.7%, and relatively lower pitch-roll cross-couplings.

All the results are obtained with one main rotor blade mode, which is the first flap mode resulting from the finite element analysis. For the BO-105 this is the first elastic flap mode, for the UH-60 it is the rigid body flap mode. Four finite elements are used in the calculation of this flap mode. The blade mass and stiffness distributions are listed in the code through lookup tables.

The present paper shows a selection of representative results. A complete set, also including trim, poles, and frequency responses will be presented in Ref. [19].

This section presents the results of a free flight simulation, carried out in hover. The results obtained with the baseline model, denoted in the plots with the "Dynamic inflow" legend, and the free wake model are compared with flight test results. The lateral cyclic input used is shown in Figure 1. Roll rate and pitch rate responses following the pitch input are shown in Figures 2 and 3 respectively. The on-axis response in roll tends to be underpredicted by the baseline model, and overpredicted when the free wake model is used. The agreement is slightly better for the free wake case, but both models reproduce the main features of the response. The off-axis response, in pitch, shows that the inability of the baseline model to predict the correct sign of the response remains even after the introduction of the free wake model.

The plots in Figures 2 and 3 show a vertical line at about 0.85 sec. This line marks the end of the second rotor revolution following the pitch input, and also the time at which some of the highest values of roll and pitch rates are reached. Any effect on wake geometry should be most visible at this time. Recall that in the simulation of a given rotor revolution the inflow distribution is that obtained from the previous revolution. No significant differences between the baseline and the free wake models appear until the third rotor revolution, when the free wake calculations show a more nose-down pitching moment than predicted by the baseline model. However, this effect is too small and occurs too late to improve the correlation with the flight test data. Whatever physical mechanisms cause the off-axis response of the helicopter to be nose-down appear to be activated within the first quarter or half of the rotor revolution during which the pitch control is applied. In this brief period of time no significant roll and pitch rates have had time to develop. This suggests two conclusions. The first is that the initial off-axis response is driven by roll or pitch *accelerations* rather than rates. The second is that the phenomenon is intrinsically unsteady, and therefore it cannot be captured by a relaxation type trailed wake model like that used in this study. This, even if the wake includes a rigorous, consistent model of geometry changes during a maneuver, and even if the maneuver itself is slow enough that a quasi-steady wake model would appear at first glance to be reasonable.

Figures 4 and 5 show respectively a rear and side view of the wake geometry during the third rotor revolution following the application of the lateral cyclic input. This geometry has been calculated by freezing all the states, and in particular the pitch and roll rate, at the value they had at the end of the second rotor revolution, which is marked by the vertical line in Figures 2 and 3. The roll and pitch rates are of about 12 deg/sec and 3 deg/sec respectively. The dashed lines in Figures 4 and 5 show the geometry of a hypothetical wake for which all the

parameters are the same as for the baseline, except for roll and pitch rates, which are set to zero. This second, "artificial" wake lacks all the effects associated with p and q, including the stretching and compressing of the trailed vortices on opposite sides of the disk due to the maneuver. The two wakes are very nearly identical, and so is the corresponding inflow distribution at the rotor disk, shown in Figures 6 and 7 for the true and the "artificial" wake respectively. This indicates that the absolute changes in wake geometry due to the maneuver are very small, which is not surprising considering that the values of roll and pitch rates are themselves quite small. The effects on the inflow of the changes in wake geometry due to the maneuver can be assessed by subtracting the inflow distribution of Figure 7 from that of Figures6. The resulting "perturbation" is shown in Figure 8. The effect of the wake geometry changes due to the maneuver is to create a downward inflow perturbation on the starboard side and an upward perturbation on the port side. This translates into lower angles of attack, lower lift, and lower flapping moments on the starboard side; the reverse is true on the port side. Because the rotor flap reaction is delayed by about 90 degrees, this in turn translates into an increase in longitudinal flapping. The conclusion is that in this case the changes in wake geometry due to the maneuver tend to increase the nose-down pitching moment acting on the helicopter. This is exactly the trend required to improve off-axis response correlation with flight test data, as Figure 3 indicates, but the magnitude of the effect is too small.

As previously mentioned, the inflow used in a given rotor revolution is that corresponding to the motion of blades and aircraft at the end of the previous revolution. This could potentially introduce artificial time delays. Therefore, the response was recalculated using the following modified update strategy. For a given rotor revolution, the integration is first carried out as before, that is, with the inflow corresponding to the motion at the end of the previous revolution. At the end of the current revolution the inflow is calculated, and with this inflow *the integration is repeated over the same revolution.* The inflow at the end of this second integration is then used for the next revolution, which is also repeated twice, and so on. This modified, "predictor-corrector-like" procedure obviously requires twice the computational effort of the baseline procedure, but it was explored to determine whether reducing the artificial time delay introduced by the baseline procedure would improve the correlation. The pitch rate response to lateral cyclic with the two different wake update procedures is shown in Figure 9. The plot clearly indicates that the wake update strategy has a negligible effect on the quality of the correlation.

The same type of coupled response, i.e., the pitch rate response to a step input of lateral cyclic, was also studied for the Sikorsky UH-60, which is equipped with an articulated rotor system. The pitch rate and the roll rate response in hover are shown respectively in Figure 10 and 10. Compared with the BO-105, the behavior of the predictions is markedly different.

For the first four rotor revolutions, corresponding to about 1 second following the maneuver, there is excellent agreement between predictions and flight test data. In particular, the model with the free wake predicts correctly the nose-down initial response, whereas the model with dynamic inflow predicts a nose-up response. The quality of the free wake predictions, however, rapidly deteriorates as time increases. This may be caused at least in part by the overprediction of the roll rate, i.e., of the *on-axis* response that is clearly visible in Figure 10. The on-axis roll frequency response plots, shown in Figure 12 show that the free wake model overpredicts the magnitude for all frequencies below 4-5 rad/sec.

The reason for the overprediction is not entirely clear. To explore whether the lack of dynamics in the free wake model could be a significant factor, the dynamic inflow model was implemented in the form

$$k[M]\dot{\lambda} + [K]\lambda = C \tag{10}$$

that is, by adding a constant k that multiplies the inflow derivative terms. This modification is simply a nonrigorous way to reduce the effect of the dynamic terms. Setting $k = 0$ would have completely eliminated inflow dynamics, but it would have turned the inflow equation, Eq. (10), into a set of algebraic equations, and the overall coupled rotor-fuselage equations into a mixed system of differential-algebraic equations, that the code is not currently equipped to handle. Therefore, a small value for k was used. The predictions for the roll rate response are shown in Figure 13: reducing inflow dynamics moves the predictions closer to that of the free wake. It should be kept in mind that the free-wake is being used here in a way that violates one of its underlying assumptions, namely that the flight condition be steady. Therefore, the use of a fully unsteady free wake model is likely to improve the correlation with flight test data for this case.

Summary and Conclusions

This paper has presented the results of a study on the effect of wake modeling on the prediction of the off-axis response to pilot inputs for a hingeless and an articulated rotor helicopter in hover. The helicopter model includes blade flexibility and a detailed description of fuselage and empennage configuration. The wake model is a relaxation type free wake, capable of modeling the geometry changes due to maneuvers. The theoretical predictions were compared with flight test results. The main conclusions of the present study are the following:

1. For the BO-105, the use of a free wake model improves only slightly the prediction of the free flight response to pilot inputs; in particular, the off-axis response is still predicted in the wrong direction, i.e., nose-up instead of nose-down for the specific

maneuver considered in the study. The effects due to the change of wake geometry during the maneuver are clearly visible, and are in the direction observed by other researchers with different wake representations. However, the magnitude of these effects is small. They can be considered contributors to the off-axis behavior of the helicopter, but not the primary driver.

2. The effects due to wake geometry changes become evident two-three rotor revolutions after the initiation of the maneuver. At that time, the actual response as observed in the flight tests has already diverged and has the opposite sign from the predictions. Indeed, these discrepancies develop after about one quarter or one half of the first rotor revolution following the maneuver, when the roll and pitch rates are negligibly small and therefore have not had time to cause appreciable changes in wake geometry. The mechanisms causing these initial discrepancies remain not fully understood. They appear to be related to pitch and roll accelerations, rather than rates.

3. The mechanisms that determine off-axis behavior seem to be especially strong over the initial portion of the first rotor revolution. If wake geometry plays a significant role, it is possible that a relaxation type, trailed free wake may not be a suitable wake model, and that a truly unsteady free wake model may be necessary. The addition of a shed wake model or, equivalently, of an unsteady aerodynamic model for the airfoil characteristics should also be explored.

4. The previous conclusions concerning the off-axis response predictions refer to the BO-105, for which the control cross-coupling effects are known to be substantial, and the off-axis rates are larger and develop more quickly than in many articulated rotor helicopters.

5. The initial off-axis response to lateral cyclic for the UH-60 is in excellent agreement with the flight test data. In particular, the error in the sign of the response is eliminated. The agreement deteriorates as time increases, probably because of the overprediction of the on-axis, i.e., roll rate response. A probable reason for the overprediction in this case is the lack of dynamics in the free wake model, which assumes steady conditions.

Acknowledgments

This research was supported by the National Rotorcraft Technology Center under the Rotorcraft Center of Excellence program. The authors would like to thank Drs. A. Bagai and J. G. Leishman for providing a copy of the maneuvering free wake code and for many useful discussions concerning its implementation, Dr. A. Desopper of ONERA for providing detailed configuration parameters for the BO-105, Dr. C. Ockier of DLR for providing the flight test data for the BO-105, and Dr. M. Tischler of the U.S. Army AFDD for providing the flight test data for the UH-60.

References

[1] Rosen, A., and Isser, A., "A Model of the Unsteady Aerodynamics of a Hovering Helicopter Rotor That Includes Variations of the Wake Geometry," *Journal of the American Helicopter Society*, Vol. 40, (3), Jul 1995, pp. 6-16.

[2] Rosen, A., and Isser, A., "A New Model of Rotor Dynamics During Pitch and Roll of a Hovering Helicopter," *Journal of the American Helicopter Society*, Vol. 40, (3), Jul 1995, pp. 17-28.

[3] Keller, J. D., "An Investigation of Helicopter Dynamic Coupling Using an Analytical Model," *Journal of the American Helicopter Society*, Vol. 41, (4), Oct 1996, pp. 322-330.

[4] Arnold, U. T. P., Keller, J. D., Curtiss, H. C., Jr., and Reichert, G., "The Effect of Inflow Models on the Predicted Response of Helicopters," *Journal of the American Helicopter Society*, Vol. 43, (1), Jan 98, pp. 25-36.

[5] Krothapalli, K. R., Prasad, J. V. R., Peters, D. A., "A Generalized Dynamic Wake Model with Wake Distortion Effects," *Proceedings of the American Helicopter Society 54th Annual Forum*, Washington, DC, May 1998.

[6] Basset, P.-M., "Modeling of the Dynamic Inflow on the Main Rotor and the Tail Components in Helicopter Flight Mechanics," Paper No. 104, *Proceedings of the 22nd European Rotorcraft Forum*, Brighton, UK, Sep 1996.

[7] Basset, P.-M., Tchen-Fo, F., "Study of the Rotor Wake Distortion Effects on the Helicopter Pitch-Roll Cross-Couplings," Paper No. FM06, *Proceedings of the 24th European Rotorcraft Forum*, Marseilles, France, Sep 1998.

[8] von Grünhagen, W., "Dynamic Inflow Modeling for Helicopter Rotors and Its Influence on the Prediction of Cross-Couplings," *Proceedings of the AHS Aeromechanics Specialists Conference*, Bridgeport, CT, October 1995.

[9] Mansur, M. H., and Tischler, M. B., "An Empirical Correction for Improving Off-Axes Responses in Flight Mechanics Helicopter Models," *Journal of the American Helicopter Society*, Vol. 43, (2), Apr 98, pp. 94-102.

[10] Rosen, A., Yaffe, R., Mansur, M. H., and Tischler, M. B., "Methods for Improving the Modeling of Rotor Aerodynamics for Flight Mechanics Purposes," *Proceedings of the American Helicopter Society 54th Annual Forum*, Washington, DC, May 1998.

[11] Bagai, A., Leishman, J. G., and Park, J., "A Free-Vortex Rotor Wake Model for Maneuvering Flight," *Proceedings of the AHS Technical Specialists' Meeting on Rotorcraft Acoustics and Aerodynamics*, Williamsburg, VA, Oct 1997.

[12] Kim, F.D., Celi, R., and Tischler, M.B., "Forward Flight Trim Calculation and Frequency Response Validation of a High-Order Helicopter Simulation Model," *Journal of Aircraft*, Vol. 30, No. 6, Nov-Dec 1993, pp. 854-863.

[13] Turnour, S. R., and Celi, R., "Modeling of Flexible Rotor Blades for Helicopter Flight Dynamic Applications," *Journal of the American Helicopter Society*, Vol. 41, No. 1, Jan 1996, pp. 52-66; Correction in Vol. 41, No. 3, Jul 1996, pp. 191-194.

[14] Turnour, S. R., and Celi, R., "Effect of Unsteady Aerodynamics on the Flight Dynamics of an Articulated Rotor Helicopter," *Journal of Aircraft*, Vol. 34, (2), Mar-Apr 1997, pp. 187-196.

[15] Peters, D.A., HaQuang, N., "Dynamic Inflow for Practical Applications", *Journal of the American Helicopter Society*, Vol. 33, (4), Oct 88, pp. 64-68.

[16] Bagai, A., and Leishman, J.G., "Rotor Free-Wake Modeling using a Pseudo-Implicit Technique—Including Comparison with Experimental Data," *Journal of the American Helicopter Society*, Vol. 40, (3), Jul 1995, pp. 29-41.

[17] Celi, R., "Hingeless Rotor Dynamics in Coordinated Turns", *Journal of the American Helicopter Society*, Vol. 36, No. 4, Oct. 1991, pp. 39-47.

[18] Chen, R.T.N., and Jeske, J.A., "Kinematic Properties of the Helicopter in Coordinated Turns," NASA Technical Paper 1773, Apr. 1981.

[19] Theodore, C., "Helicopter Flight Dynamics Simulation Modeling Including Refined Aerodynamics," Ph.D. Dissertation, Department of Aerospace Engineering, University of Maryland, College Park, December 1999.

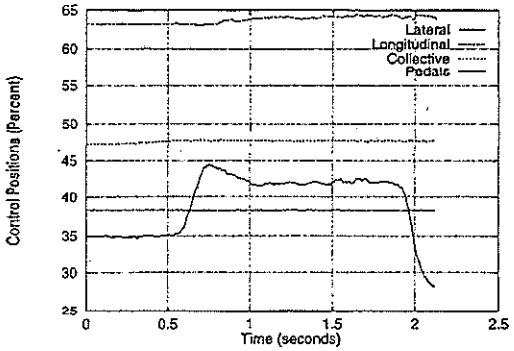

Figure 1: Lateral cyclic input.

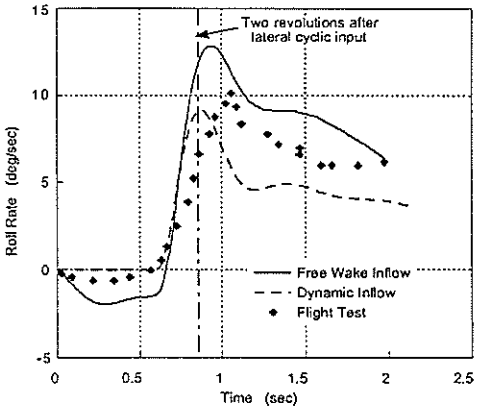

Figure 2: Roll rate after application of lateral cyclic input.

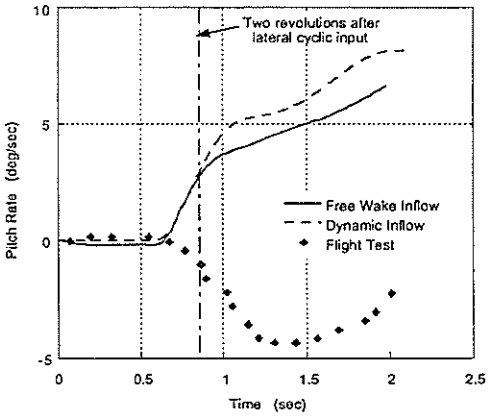

Figure 3: Pitch rate after application of lateral cyclic input.

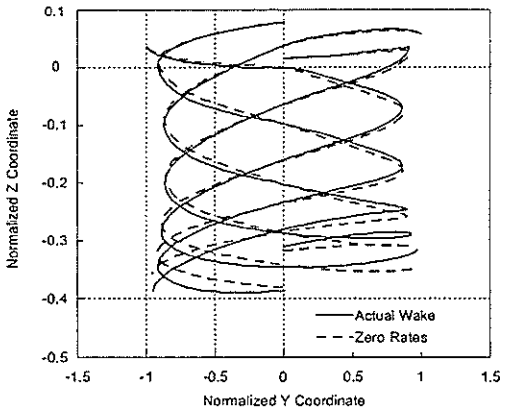

Figure 4: Wake geometry after approximately two revolutions from pitch input; rear view.

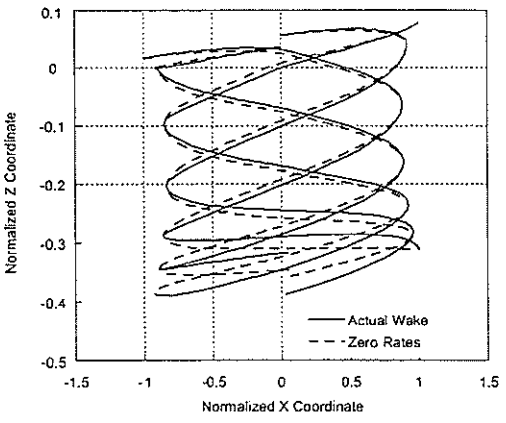

Figure 5: Wake geometry after approximately two revolutions from pitch input; side view.

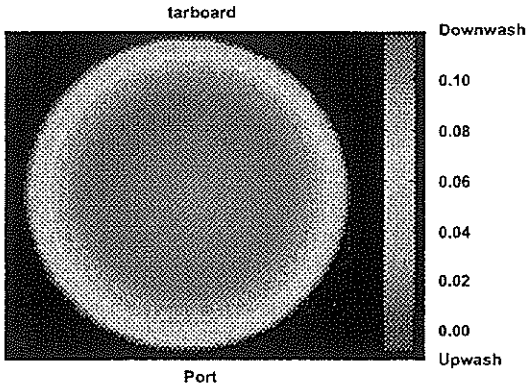

Figure 6: Inflow distribution after approximately two revolutions from pitch input; free wake.

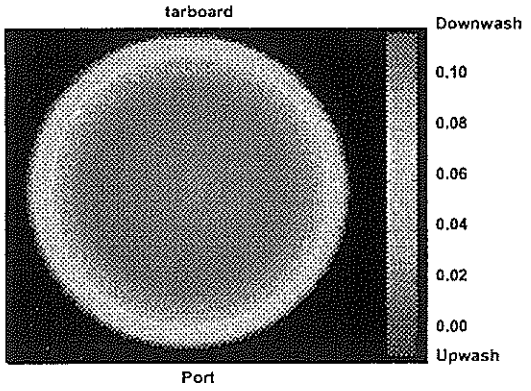

Figure 7: Inflow distribution after approximately two revolutions from pitch input; free wake with $p = q = 0$.

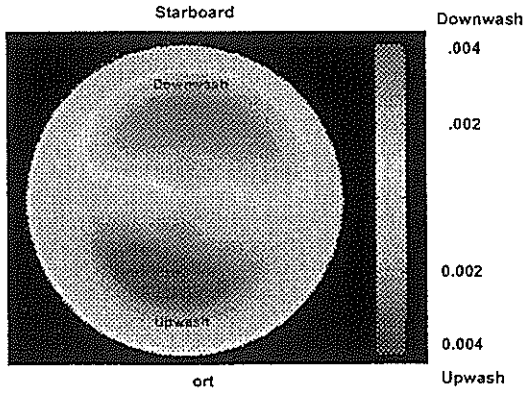

Figure 8: Inflow distribution after approximately two revolutions from pitch input; difference between true free wake and free wake with $p = q = 0$.

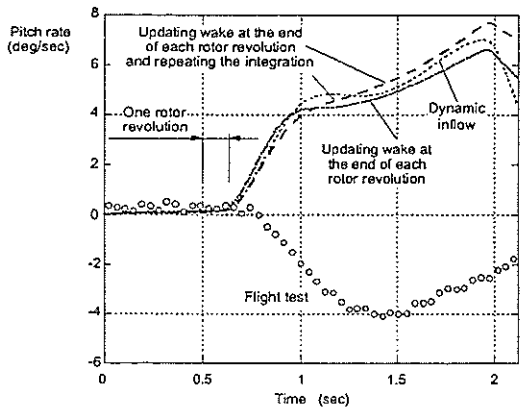

Figure 9: Time histories with two different wake update procedures, BO-105.

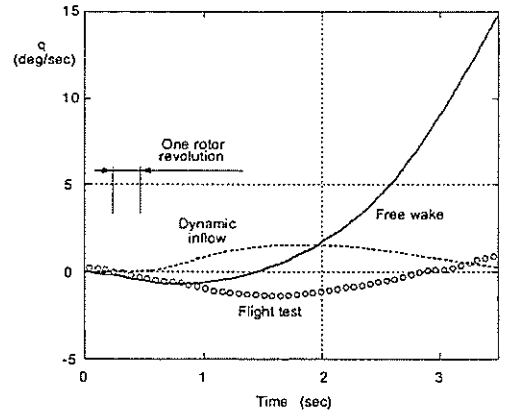

Figure 10: Pitch rate after application of lateral cyclic input, UH-60.

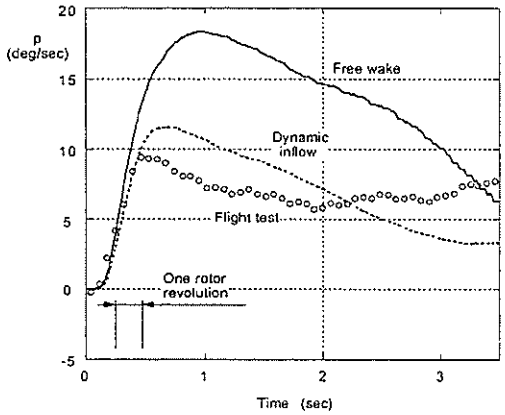

Figure 11: Roll rate after application of lateral cyclic input, UH-60.

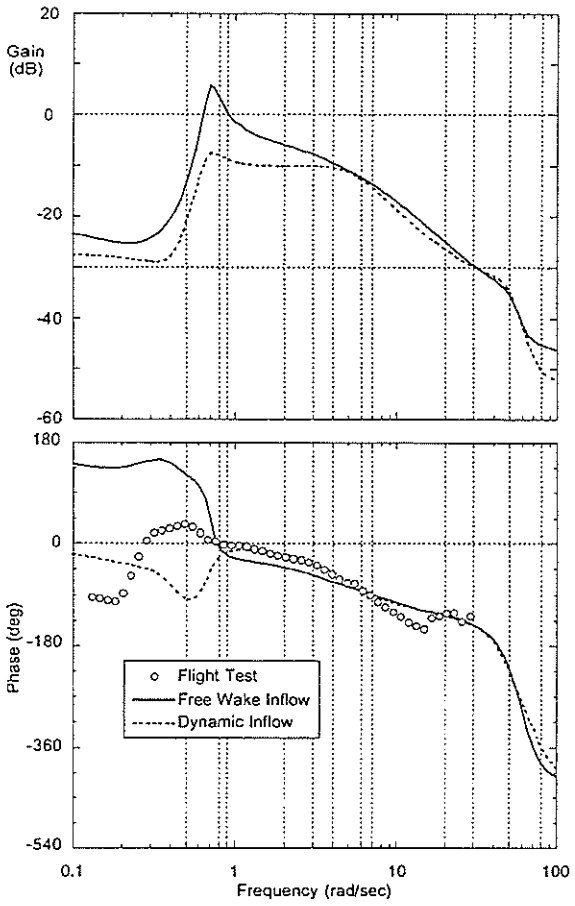

Figure 12: On axis roll frequency response, UH-60.

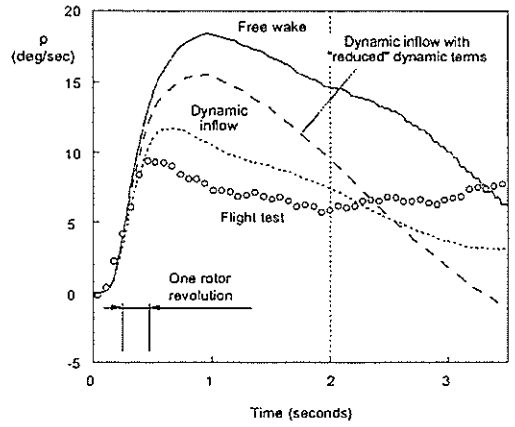

Figure 13: Effect of wake dynamics on on-axis roll response prediction, UH-60 in hover.